V European Conference on Computational Fluid Dynamics
ECCOMAS CFD 2010
J. C. F. Pereira and A. Sequeira (Eds)
Lisbon, Portugal,14-17 June 2010

ON THE USE OF HIGH ORDER COMPACT SCHEMES FOR THE SIMULATION OF STABLY STRATIFIED FLUID FLOW

Tomáš Bodnár[*,‡], Philippe Fraunié[†], Karel Kozel[‡]

[*]Czech Technical University, Faculty of Mechanical Engineering, Department of Technical Mathematics
Karlovo Náměsti 13, 121 35 Prague 2, Czech Republic
e-mail: Tomas.Bodnar@fs.cvut.cz

[†]Université du Sud Toulon-Var, Laboratoire de Sondages Electromagnétiques de l'Environnement Terrestre
Bâtiment F, BP 132, 83957 La Garde Cedex, France
e-mail: philippe.fraunie@lseet.univ-tln.fr

[‡]Academy of Sciences of the Czech Republic, Institute of Thermomechanics
Dolejškova 1402/5, 182 00 Prague 8, Czech Republic
e-mail: kozelk@fsik.cvut.cz

Key words: stratification, finite-difference, compact scheme, Runge-Kutta, Boussinesq approximation,

Abstract. *The aim of this paper is to present the class of high order compact schemes in the context of numerical simulation of stratified flow. The numerical schemes presented here are based on the approach outlined in*[1]*. Up to now, these very high order schemes have successfully been applied to various problems namely in the area of computational aeroacoustics where they have shown outstanding accuracy, and favorable diffusion/dispersion properties.*

The numerical model presented in this contribution is based on the solution of the Boussinesq approximation by a finite-difference scheme. The numerical scheme itself follows the principle of semi-discretization, with high order compact discretization in space, while the time integration is carried out by suitable Runge-Kutta time-stepping scheme. In the case presented here the steady flow was considered and thus the artificial compressibility method was used to resolve the pressure from the modified continuity equation.

The test case used to demonstrate the capabilities of the selected model consists of the flow of stably stratified fluid over low, smooth hill. This case was chosen to simulate the common situation appearing in the atmospheric boundary layer flows over orography.

1 INTRODUCTION

The stratified fluid flows appear in many areas of applied physics. The work presented hereafter is motivated by air flow in the atmospheric boundary layer, where the atmospheric stability conditions have a crucial influence on flow and consequently also on pollution dispersion. In this work the stably stratified case is solved, searching for typical artifacts of this kind of flow. One of the well known effects of stably stratified flow over hills is generation of wave patterns in the flow field. These waves affect large areas surrounding the hill both in downwind and upwind direction. The effect of orography could thus be felt in much larger area than in the case of neutral stratification.

The correct numerical resolution of the flow-field in this case is very demanding concerning the choice of the numerical discretization. Such numerical discretization should have well controlled numerical diffusion/dispersion properties on one hand and on the other hand should be simple enough to allow for solution of large scale problems occurring in the atmospheric physics. This was the major reason that led us to the choice of high order compact finite-difference space discretization and strong stability preserving time-integration methods for the present study.

The results presented herein were obtained using the first generation of the numerical code, which serves us as a technological demonstrator to verify the capabilities of the selected numerical methods. Numerical simulations were carried out on a simple 2D case for laminar flow. We were looking for qualitative behavior of the solution for various levels of stratification.

2 MATHEMATICAL MODEL

2.1 Full incompressible model

The motion equations describing the flow of incompressible fluid could be written in the following general form (1) and (2). Here we assume that the energy equation is decoupled from the equations of motion and the consequences of this simplification could be neglected. This e.g. means that heat production due to the mechanical energy dissipation and the density change related to temperature variations are neglected..

$$\frac{\partial \rho}{\partial t} + \mathrm{div}(\rho \boldsymbol{u}) = 0 \tag{1}$$

$$\frac{\partial \rho \boldsymbol{u}}{\partial t} + \mathrm{div}(\rho \boldsymbol{u} \otimes \boldsymbol{u}) = \mathrm{div}\mathbb{S} + \rho \boldsymbol{f} \tag{2}$$

Here $\boldsymbol{u} = (u, v, w)$ is the velocity vector in coordinate system (x, y, z). Pressure is denoted by p, density by ρ. These equations together with the incompressibility constrain $\mathrm{div}\boldsymbol{u} = 0$ and the constitutive relation for the stress tensor for Newtonian incompressible fluid $\mathbb{S} = -p\mathbb{I} + 2\mu\mathbb{D}$ and gravity force expressed as $\boldsymbol{f} = (0, 0, g)$ leads (exactly) to the following

set of governing equations for unknowns $\boldsymbol{u}$, p and ρ:

$$\frac{\partial u}{\partial x}+\frac{\partial v}{\partial y}+\frac{\partial w}{\partial z} = 0 \tag{3}$$

$$\frac{\partial \rho}{\partial t}+\frac{\partial(\rho u)}{\partial x}+\frac{\partial(\rho v)}{\partial y}+\frac{\partial(\rho w)}{\partial z} = 0 \tag{4}$$

$$\frac{\partial(\rho u)}{\partial t}+\frac{\partial(\rho u^2+p)}{\partial x}+\frac{\partial(\rho uv)}{\partial y}+\frac{\partial(\rho uw)}{\partial z} = \mu\Delta u \tag{5}$$

$$\frac{\partial(\rho v)}{\partial t}+\frac{\partial(\rho uv)}{\partial x}+\frac{\partial(\rho v^2+p)}{\partial y}+\frac{\partial(\rho vw)}{\partial z} = \mu\Delta v \tag{6}$$

$$\frac{\partial(\rho w)}{\partial t}+\frac{\partial(\rho uw)}{\partial x}+\frac{\partial(\rho vw)}{\partial y}+\frac{\partial(\rho w^2+p)}{\partial z} = \mu\Delta w+\rho g \tag{7}$$

This system could alternatively be rewritten in an equivalent form:

$$\frac{\partial u}{\partial x}+\frac{\partial v}{\partial y}+\frac{\partial w}{\partial z} = 0 \tag{8}$$

$$\frac{\partial \rho}{\partial t}+\frac{\partial(\rho u)}{\partial x}+\frac{\partial(\rho v)}{\partial y}+\frac{\partial(\rho w)}{\partial z} = 0 \tag{9}$$

$$\rho\left(\frac{\partial u}{\partial t}+\frac{\partial(u^2+p)}{\partial x}+\frac{\partial(uv)}{\partial y}+\frac{\partial(uw)}{\partial z}\right) = \mu\Delta u \tag{10}$$

$$\rho\left(\frac{\partial v}{\partial t}+\frac{\partial(uv)}{\partial x}+\frac{\partial(v^2+p)}{\partial y}+\frac{\partial(vw)}{\partial z}\right) = \mu\Delta v \tag{11}$$

$$\rho\left(\frac{\partial w}{\partial t}+\frac{\partial(uw)}{\partial x}+\frac{\partial(vw)}{\partial y}+\frac{\partial(w^2+p)}{\partial z}\right) = \mu\Delta w+\rho g \tag{12}$$

2.2 Boussinesq approximation

Now assuming that the pressure and density fields are perturbation of hydrostatic equilibrium state, i.e.:

$$\rho(x,y,z,t) = \rho_0(z)+\rho'(x,y,z,t) \tag{13}$$

$$p(x,y,z,t) = p_0(z)+p'(x,y,z,t) \tag{14}$$

and

$$\frac{\partial p_0}{\partial z} = \rho_0 g \tag{15}$$

The Boussinesq approximation is obtained by introducing the above relations into the momentum equations (10), (11) and (12), where the density perturbation ρ' is neglected on the left-hand side while on the right-hand side it is retained.

$$\frac{\partial u}{\partial x}+\frac{\partial v}{\partial y}+\frac{\partial w}{\partial z} = 0 \tag{16}$$

$$\frac{\partial \rho'}{\partial t} + \frac{\partial(\rho' u)}{\partial x} + \frac{\partial(\rho' v)}{\partial y} + \frac{\partial(\rho' w)}{\partial z} = -w\frac{\partial \rho_0}{\partial z} \tag{17}$$

$$\frac{\partial u}{\partial t} + \frac{\partial(u^2)}{\partial x} + \frac{\partial(uv)}{\partial y} + \frac{\partial(uw)}{\partial z} = \frac{1}{\rho_0}\left(-\frac{\partial p'}{\partial x} + \mu\Delta u\right) \tag{18}$$

$$\frac{\partial v}{\partial t} + \frac{\partial(uv)}{\partial x} + \frac{\partial(v^2)}{\partial y} + \frac{\partial(vw)}{\partial z} = \frac{1}{\rho_0}\left(-\frac{\partial p'}{\partial y} + \mu\Delta v\right) \tag{19}$$

$$\frac{\partial w}{\partial t} + \frac{\partial(uw)}{\partial x} + \frac{\partial(vw)}{\partial y} + \frac{\partial(w^2)}{\partial z} = \frac{1}{\rho_0}\left(-\frac{\partial p'}{\partial z} + \mu\Delta w + \rho' g\right) \tag{20}$$

This system could equivalently be rewritten using the "complete" density ρ rather than the perturbation ρ'.

$$\frac{\partial u}{\partial x} + \frac{\partial v}{\partial y} + \frac{\partial w}{\partial z} = 0 \tag{21}$$

$$\frac{\partial \rho}{\partial t} + \frac{\partial(\rho u)}{\partial x} + \frac{\partial(\rho v)}{\partial y} + \frac{\partial(\rho w)}{\partial z} = 0 \tag{22}$$

$$\frac{\partial u}{\partial t} + \frac{\partial(u^2)}{\partial x} + \frac{\partial(uv)}{\partial y} + \frac{\partial(uw)}{\partial z} = \frac{1}{\rho_0}\left(-\frac{\partial p'}{\partial x} + \mu\Delta u\right) \tag{23}$$

$$\frac{\partial v}{\partial t} + \frac{\partial(uv)}{\partial x} + \frac{\partial(v^2)}{\partial y} + \frac{\partial(vw)}{\partial z} = \frac{1}{\rho_0}\left(-\frac{\partial p'}{\partial y} + \mu\Delta v\right) \tag{24}$$

$$\frac{\partial w}{\partial t} + \frac{\partial(uw)}{\partial x} + \frac{\partial(vw)}{\partial y} + \frac{\partial(w^2)}{\partial z} = \frac{1}{\rho_0}\left(-\frac{\partial p'}{\partial z} + \mu\Delta w + (\rho - \rho_0)g\right) \tag{25}$$

3 NUMERICAL METHODS

3.1 Space discretization

The spatial discretization used in this work is directly based on the paper *Lele* [2], where the class of very high order compact finite difference schemes was introduced and analyzed. The main idea used to construct this family of schemes is that instead of approximating the spatial derivatives ϕ' of certain quantity ϕ explicitly from the neighboring values ϕ_i, the (symmetric) linear combination of neighboring derivatives $(\ldots, \phi'_{i-1}, \phi'_i, \phi'_{i+1}, \ldots)$ is approximated by weighted average of central differences.

The simplest compact finite difference schemes use the approximation in the form

$$a\,\phi'_{i-1} + \phi'_i + a\,\phi'_{i+1} = \alpha_1\frac{\phi_{i+1} - \phi_{i-1}}{2h} + \alpha_2\frac{\phi_{i+2} - \phi_{i-2}}{4h} \tag{26}$$

Here $h = x_i - x_{i-1}$ is the spatial step, while a and α_k are the coefficients determining the specific scheme within the family described by (26).

This approach generalizes the classical finite-differencing, which now becomes just a special case of the compact approach for $a = 0$.

It is evident that the schemes (26) form a subclass of three-diagonal schemes with five-point computational stencil. For the simulations presented here, the following coefficients were used

$$\alpha_1 = \frac{2}{3}(a+2) \qquad \alpha_2 = \frac{1}{3}(4a-1) \tag{27}$$

The parameter $a = 5/14$ was used within this study, which leads to a formally fourth order accurate scheme. Other choices of parameters are possible, leading to schemes up to order six (for $a = 1/3$).

The above presented schemes are based on central discretization in space with all the well known advantages and also disadvantages of this class of methods. One of the disadvantages the central methods is the occurrence of non-physical oscillations in the numerical approximations. A very efficient algorithm for filtering out these high frequency oscillations was also proposed in *Lele* [2]. The low-pass filter (for the filtered values $\widehat{\phi}_i$ could be formulated in a form very similar to (26):

$$b\,\widehat{\phi}_{i-1} + \widehat{\phi}_i + b\,\widehat{\phi}_{i+1} = 2\beta_0\phi_i + \beta_1\frac{\phi_{i+1}+\phi_{i-1}}{2h} + \beta_2\frac{\phi_{i+2}+\phi_{i-2}}{4h} + \beta_3\frac{\phi_{i+3}+\phi_{i-3}}{6h} \tag{28}$$

The filters of different orders could be obtained vor various choices of coefficients. Here the fourth order filter with coefficients

$$\beta_0 = \frac{1}{8}(3b+10) \qquad \beta_1 = \frac{1}{2}(2b+1) \qquad \beta_2 = \frac{1}{8}(2b-1) \qquad \beta_3 = 0 \tag{29}$$

was used. The parameter $0 < b < 0.5$ is used to fine-tune the filter.

More details on the space discretization can be found in *Lele* [2], *Visbal & Gaitonde* [5], *Gaitonde et al.* [1].

3.2 Temporal discretization

The system of governing Partial Differential Equations was discretized in space using the above described finite-difference technique (represented further by the space discretization operator $\widetilde{\mathcal{L}}$). This leads to a system of Ordinary Differential Equations for time-evolution of grid values of the vector of unknowns W. This concept is called semi-discretization or the method of lines. Resulting system of ODE's could be solved by a suitable time-integration method. In this study we have used the so called Strong Stability Preserving Runge-Kutta methods.

The family of explicit SSP Runge-Kutta schemes is usually written in the form introduced in *Shu & Osher* [3].

$$\begin{aligned} \mathsf{W}^{(0)} &= \mathsf{W}^n \\ \mathsf{W}^{(r)} &= \sum_{p=0}^{r-1}\Big(\alpha_{rp}\mathsf{W}^{(p)} + \beta_{rp}\Delta t\widetilde{\mathcal{L}}(\mathsf{W}^{(p)})\Big) \qquad r = 1,\ldots,s \\ \mathsf{W}^{n+1} &= \mathsf{W}^{(s)} \end{aligned} \tag{30}$$

It is not difficult to see that in the case the coefficients β_{rp} are positive, the method (30) is nothing but a convex combination of Euler stages with fractional time-steps of the length $\frac{\beta_{rp}}{\alpha_{rp}}\Delta t$.

Here we just shortly present some of the optimal, in the sense of accuracy versus stability, up to the order three SSP RK methods, originally studied in[4]. Hereafter the SSP(s,o) denotes the Runge-Kutta method which consists of s stages and has order of accuracy o.

Method	α_{rp}			β_{rp}			CFL
SSP(1,1)	1			1			1
SSP(2,1)	1			$\frac{1}{2}$			2
	0	1		0	$\frac{1}{2}$		
SSP(3,1)	1			$\frac{1}{3}$			3
	0	1		0	$\frac{1}{3}$		
	0	0	1	0	0	$\frac{1}{3}$	

Table 1: First order SSP-RK methods coefficients

The method denoted by SSP(1,1) is nothing but the Euler method, while SSP(2,2) stands for the modified Euler method. The coefficients of higher (second and third) order SSP-RK methods can be found in[4].

Method	α_{rp}				β_{rp}				CFL
SSP(2,2)	1				1				1
	$\frac{1}{2}$	$\frac{1}{2}$			0	$\frac{1}{2}$			
SSP(3,2)	1				$\frac{1}{2}$				2
	0	1			0	$\frac{1}{2}$			
	$\frac{1}{3}$	0	$\frac{2}{3}$		0	0	$\frac{1}{3}$		
SSP(4,2)	1				$\frac{1}{3}$				3
	0	1			0	$\frac{1}{3}$			
	0	0	1		0	0	$\frac{1}{3}$		
	$\frac{1}{4}$	0	0	$\frac{3}{4}$	0	0	0	$\frac{1}{4}$	

Table 2: Second order SSP-RK methods coefficients

The table 2 shows that the higher order of RK method could only be achieved at the expense of the reduction of the allowable time-step, resp. the CFL.

The three stage second order SSP Runge-Kutta method was used to obtain the results presented here.

4 NUMERICAL SIMULATIONS

4.1 Computational domain

The 2D computational domain is selected as a part of wall-bounded half space with low smooth cosine-shaped hill. The hill height is $h = 1m$, while the whole domain has dimensions $90 \times 30\, m$.

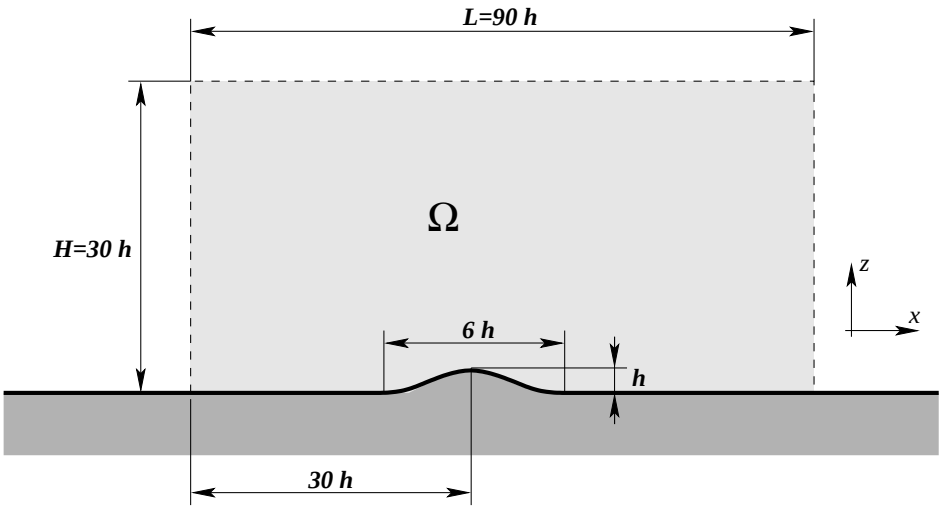

Figure 1: Computational domain configuration

4.2 Boundary conditions

Two-dimensional case is considered and thus only boundary conditions are given for this 2D case.

- **Inlet** ... The velocity profile $\boldsymbol{u} = (u(z), 0, 0)$ is prescribed. The horizontal velocity component u is given by $u(z) = U_0(z/H)^{1/r}$ with $U_0 = 1m/s$ and $r = 40$. Density perturbation ρ' is set to zero, while homogeneous Neumann condition is used for pressure.

- **Outlet** ... Homogeneous Neumann condition is prescribed for all velocity components, as well as for the pressure and density perturbations.

- **Wall** ... No-slip conditions are used on the wall, i.e. the velocity vector is set to $\boldsymbol{u} = (0, 0, 0)$. Homogeneous Neumann condition is used for pressure and density perturbations.

- **Free stream** ... Homogeneous Neumann condition is used for all quantities including pressure and density perturbations.

The background density field is given by $\rho_0(z) = \rho_w + \gamma z$ with $\rho_w = 1.2\, kg \cdot m^{-3}$ and $\gamma = -0.01\, kg \cdot m^{-4}$. A range of gravity acceleration g was used to test the behavior of the model and numerical method for different Brunt-Väisälä frequencies. The values used are $g = 0,\ -2,\ -5,\ -10,\ -20,\ -50\, m \cdot s^{-2}$.

4.3 Computational grid

The numerical simulations were performed on a structured, non-orthogonal wall-fitted grid shown in the figure 2. The grid has 152×68 points with the minimum cell size in the near-wall region $\Delta z = 0.03m$

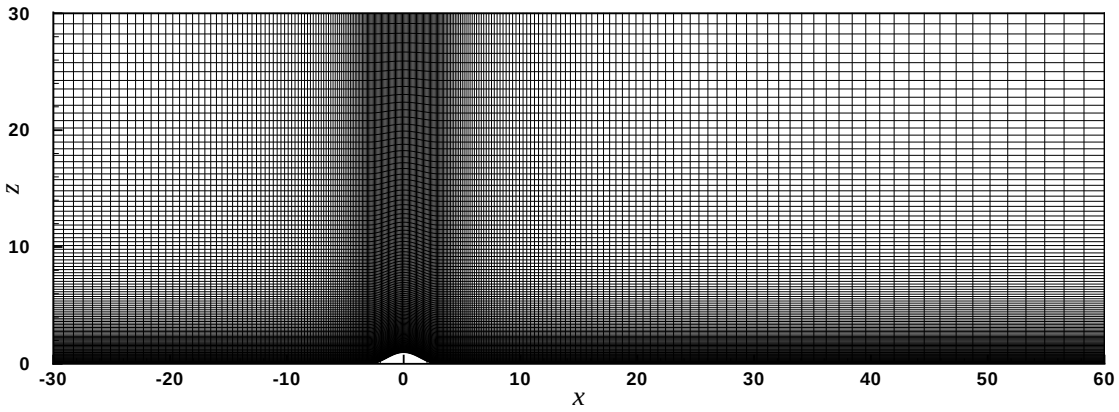

Figure 2: Computational grid

4.4 Numerical results

The figure 3 shows the comparison of horizontal velocity contours for six different values of g. The first image in the series corresponds to the reference case where no gravity force is applied. The zone of reversal flow is marked by white contour color. As expected the increase of the (absolute) value of g leads to the more pronounced wave patterns in the proximity of the hill. The wavelength of the waves decreases as it should based on the

definition of Brunt-Väisälä frequency

$$N = \sqrt{-\frac{g}{\bar{\rho}} \frac{\partial \rho_0}{\partial z}} \tag{31}$$

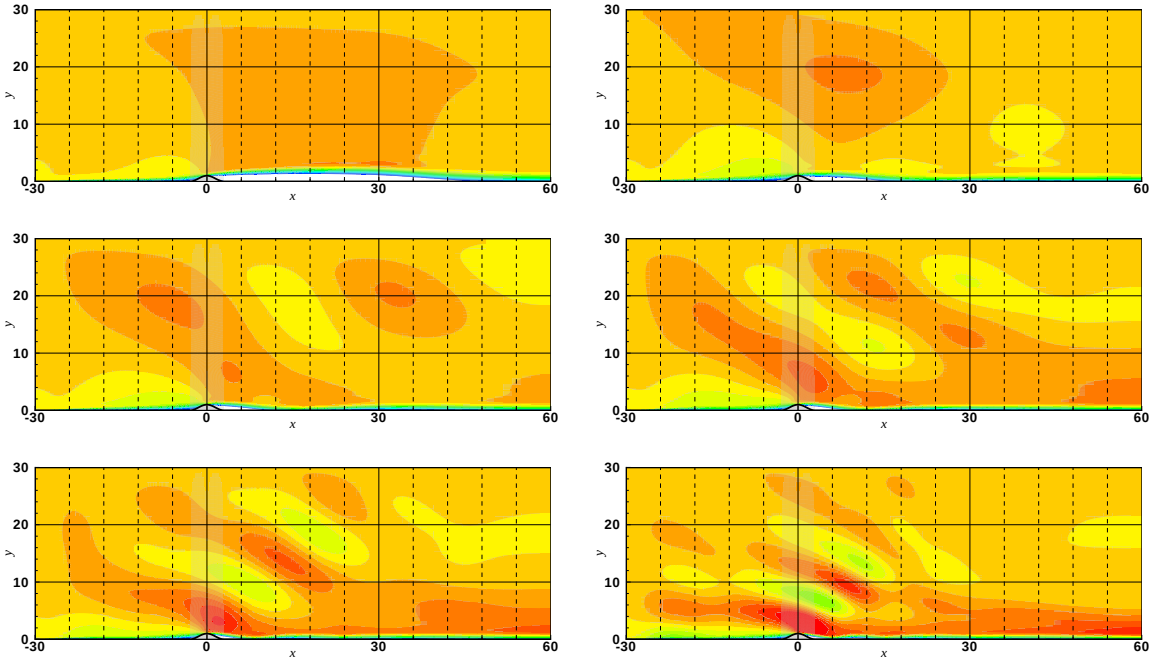

Figure 3: Contours of the horizontal velocity for $g = 0,\ -2,\ -5,\ -10,\ -20,\ -50\, m \cdot s^{-2}$

The stabilizing effect of the stratification is also visible in shortening of the recirculation zone behind the hill.

5 CONCLUSIONS

- The mathematical model produced results that are in good qualitative agreement with our expectations.
- The implementation of the selected numerical methods seems to work properly and is free of obvious errors.
- Future work will concentrate on exploration of full capabilities of numerical method.
- More effort will be needed to extend the numerical solver for complex more realistic geometries.

Acknowledgement: The financial support for this work was provided by the Research Plan *MSM 6840770010* of the Ministry of Education of Czech Republic.

References

[1] Gaitonde, D. V., Shang, J. S., & Young, J. L.: Practical aspects of higher-order numerical schemes for wave propagation phenomena. *International Journal for Numerical Methods in Engineering*, vol. 45: (1999) pp. 1849–1869.

[2] Lele, S. K.: Compact Finite Difference Schemes with Spectral-like Resolution. *Journal of Computational hysics*, vol. 103: (1992) pp. 16–42.

[3] Shu, C. W. & Osher, S.: Efficient implementation of essentially non-oscillatory shock-capturing schemes. *Journal of Computational Physics*, vol. 77: (1988) pp. 439–471.

[4] Spiteri, R. J. & Ruuth, S. J.: A new class of optimal high-order strong-stability-preserving time discretization methods. *SIAM Journal on Numerical Analysis*, vol. 40, no. 2: (2002) pp. 469–491.

[5] Visbal, M. R. & Gaitonde, D. V.: On the Use of Higher-Order Finite-Difference Schemes on Curvilinear and Deforming Meshes. *Journal of Computational Physics*, vol. 181: (2002) pp. 155–185.